Electronic Supplementary Material (ESI) for Chemical Science.

Supramolecular anion recognition in water: synthesis of hydrogen-bonded supramolecular frameworks

Mahbod Morshedi,[a] Michael Thomas,[a] Andrew Tarzia,[b]

Christian J. Doonan,[b] and Nicholas G. White[a]*

[a]*Research School of Chemistry, Australian National University*

137 Sullivan's Creek Road, Acton, 2601, ACT, Australia

Email: nicholas.white@anu.edu.au

URL: www.nwhitegroup.com

[b]*Department of Chemistry and Centre for Advanced Materials, School of Physical Sciences, The University of Adelaide, Adelaide, 5005, SA, Australia*

Contents

Experimental considerations and details of instrumentation

THF was dried by distilling from sodium/benzophenone. $TBA_2 \cdot TP$ was prepared by a slight modification of the method described by Pfeffer.[S1] Tetra(4-cyanophenyl)methane was prepared in two steps from tetraphenylmethane as described by Hoskins and Robson.[S2] While tetraphenylmethane is commercially-available, it is relatively expensive, and so it was prepared in two steps from triphenylmethyl chloride, as described by Zimmerman and Müller.[S3] Model compound **1·Cl** was prepared from commercially-available *tert*-butyl-benzonitrile as described by Lehn.[S4] All other chemicals were purchased from commercial suppliers and used as received.

NMR spectra were collected on Varian Gemini, Bruker Avance 400 or Bruker Avance 700 spectrometers and are referenced to the residual solvent signal.[S5] Infrared spectra were recorded on a Perkin-Elmer Spectrum Two FT-IR Spectrometer fitted with an ATR Two Single Reflection Diamond. Thermogravimetric analyses were recorded on a TA Instruments Q500 analyser.

Details of instruments used to record ITC, PXRD and SCXRD data are given in the respective sections of the Supporting Information.

Synthesis and characterisation

Synthesis of 1·BPh₄

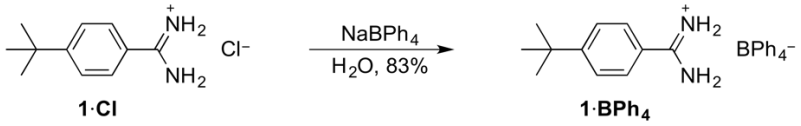

1·Cl **1·BPh₄**

Scheme S1. Synthesis of **1·BPh₄**.

1·BPh₄

A solution of sodium tetraphenylborate (0.137 g, 0.400 mmol) in water (5 mL) was added to a solution of **1·Cl** (0.0426 g, 0.200 mmol) in water (5 mL) causing the immediate formation of a precipitate. This was isolated by filtration, washed with water (3 × 5 mL) and dried *in vacuo* to give **1·BPh₄** as a white powder. Yield: 0.0818 g (0.165 mmol, 83%).

^{1}H NMR (d$_6$-DMSO): δ 8.99 (br. s, 4H), 7.74 (d, *J* = 8.4 Hz, 2H), 7.64 (d, *J* = 8.4 Hz, 2H), 7.17 (br. s, 8H), 6.92 (t, *J* = 7.3 Hz, 8 H), 6.78 (t, *J* = 7.2 Hz, 4H), 1.32 (s, 9H) ppm.

^{13}C NMR (d$_6$-DMSO): δ 165.3, 162.6–164.1 (m), 157.0, 135.5, 128.0, 125.8, 125.2, 121.5, 34.9, 30.7 ppm.

LRESI-MS (pos.): 177.2, calc. for $[C_{11}H_{17}N_2]^+$ (*i.e.* loss of BPh_4^-) = 177.1

673.8; calc. for $[(C_{11}H_{17}N_2)_2{\cdot}(C_{24}H_{20}{}^{11}B)]^+$ = 673.4

LRESI-MS (neg.): 319.2, calc. for $[C_{24}H_{20}{}^{11}B]^-$ (*i.e.* BPh_4^-) = 319.2 Da.

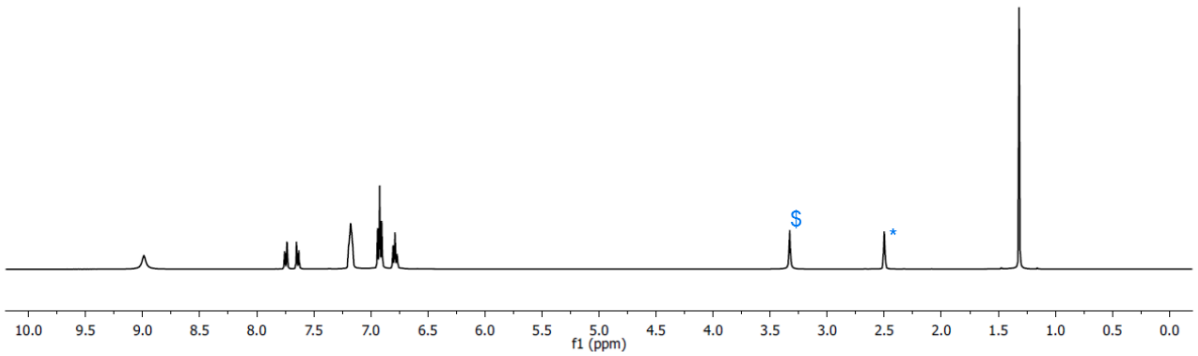

Figure S1. ^{1}H NMR spectrum of **1·BPh₄** (400 MHz, 298 K, d$_6$-DMSO, peak marked * corresponds to residual solvent signal, peak marked $ corresponds to water).

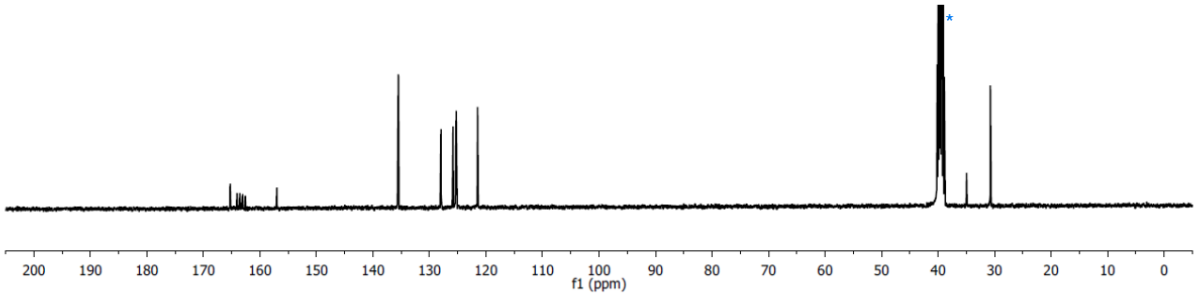

Figure S2. ^{13}C NMR spectrum of **1·BPh₄** (100 MHz, 298 K, d$_6$-DMSO, peak marked * corresponds to residual solvent signal).

Synthesis of 2·4Cl, 2·4BPh₄, 2·4Br and 2·4NO₃

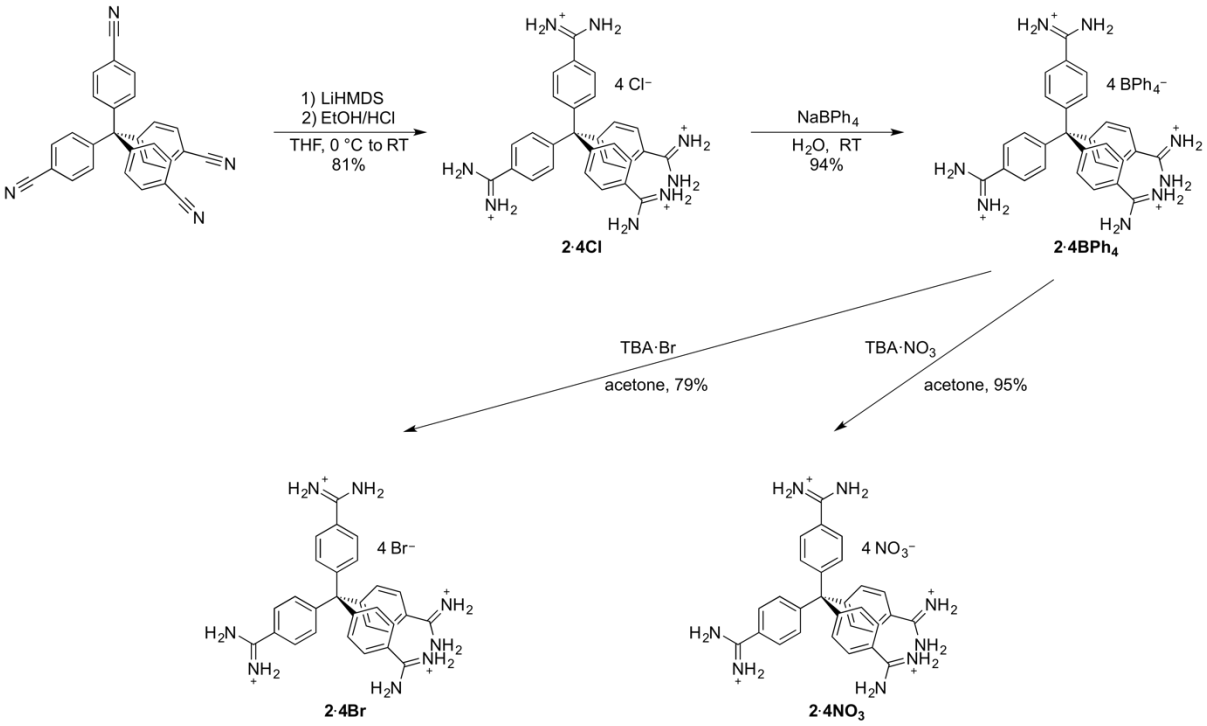

Scheme S2. Synthesis of **2·4Cl**,**2·4BPh₄**, **2·4Br** and **2·4NO₃**.

The synthesis of **2·4Cl** is described in the main article.

2·4Cl has only limited solubility in DMSO, but a ^{1}H NMR spectrum (Figure S3) was collected in this solvent to check that all NH_4Cl, which is produced by quenching LiHMDS with acid, had been removed from the product. If present, NH_4^+ is clearly visible as a triplet with J ~ 50 Hz at approx. 7.3 ppm in d_6-DMSO.

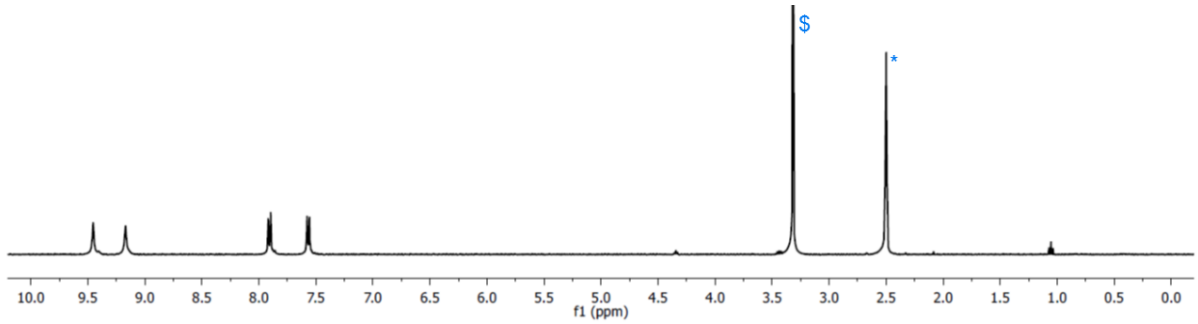

Figure S3. ^{1}H NMR spectrum of **2·4Cl**·(400 MHz, 298 K, d_6-DMSO, peak marked * corresponds to residual solvent signal, peak marked $ corresponds to water). *Note: spectrum is of relatively low quality due to the low solubility of **2·4Cl** in DMSO; see note on previous page, and Figure S4 for a better quality spectrum.*

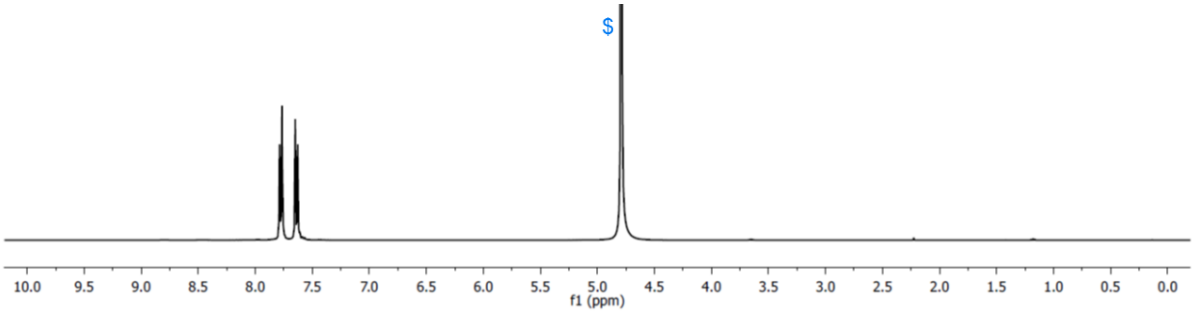

Figure S4. ^{1}H NMR spectrum of **2·4Cl** (400 MHz, 298 K, D_2O, peak marked $ corresponds to water).

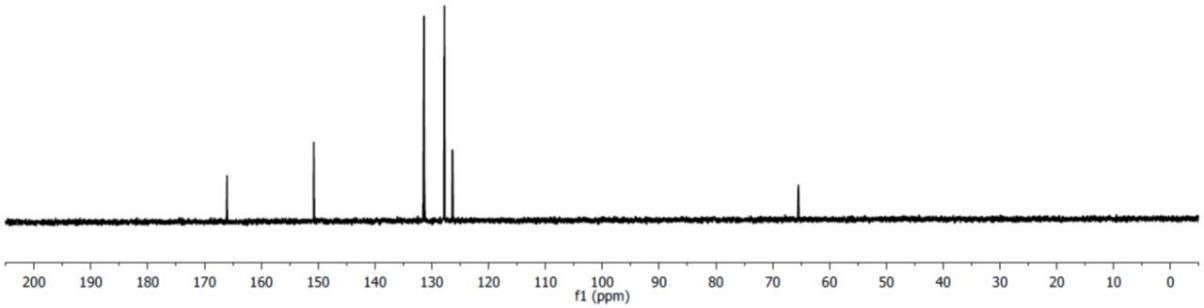

Figure S5. ^{13}C NMR spectrum of **2·4Cl** (100 MHz, 298 K, D_2O).

2·4BPh$_4$

A solution of sodium tetraphenylborate (0.113 g, 0.331 mmol) in water (10 mL) was added to a solution of **2·4Cl** (0.0500 g, 0.0788 mmol) in water (5 mL) causing the immediate formation of a precipitate. This was isolated by filtration, washed with water (3 × 5 mL), and dried *in vacuo* to give **2·4BPh$_4$** as a white powder. Yield: 0.132 g (0.0746 mmol, 94%).

^{1}H NMR (d$_6$-DMSO): δ 8.55 (br. s, 16H), 7.81 (d, *J* = 8.2 Hz, 8H), 7.57 (d, *J* = 8.2 Hz, 8H), 7.18 (br. s, 48H), 6.93 (t, *J* = 7.3 Hz, 48H) 6.79 (t, *J* = 7.3 Hz, 24H) ppm.

^{13}C NMR (d$_6$-DMSO): δ 162.6–164.5 (m), 150.4, 135.6, 130.4, 128.4, 126.4, 125.4, 121.6, 65.4 ppm.

LRESI-MS (pos.): 809.3, calc. for $[C_{53}H_{50}N_8B]^+$ (*i.e.* loss of 2 H^+ and 3 BPh_4^-) = 809.4

489.4, calc. for $[C_{29}H_{29}N_8]^+$ (*i.e.* loss of 3 H^+ and 4 BPh_4^-) = 489.3

245.2, calc. for $[C_{29}H_{30}N_8]^{2+}$ (*i.e.* loss of 2 H^+ and 4 BPh_4^-) = 245.1

LRESI-MS (neg.): 319.3, calc. for $[C_{24}H_{20}{}^{11}B]^-$ (*i.e.* BPh_4^-) = 319.2 Da.

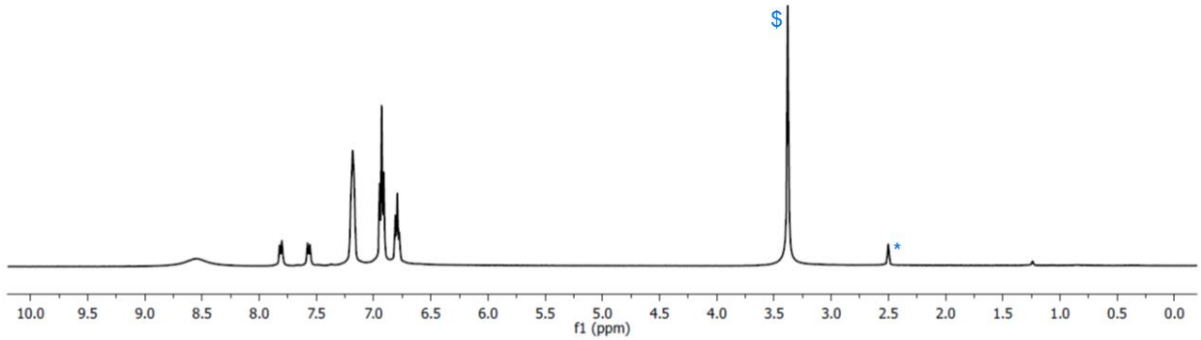

Figure S6. ^{1}H NMR spectrum of **2·4BPh$_4$** (400 MHz, 298 K, d$_6$-DMSO, peak marked * corresponds to residual solvent signal, peak marked $ corresponds to water).

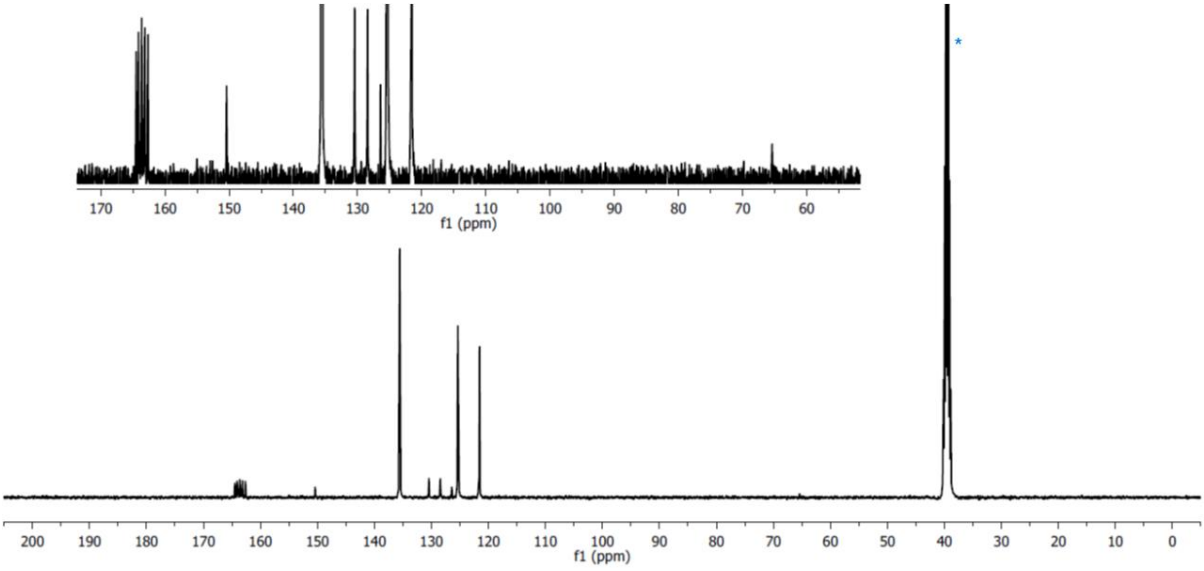

Figure S7. ^{13}C NMR spectrum of **2·4BPh$_4$** (100 MHz, 298 K, d$_6$-DMSO, peak marked * corresponds to residual solvent signal).

2·4Br

A solution of TBA·Br (0.500 g, 1.55 mmol) in acetone (5 mL) was added to a solution of **2·4BPh$_4$** (0.280 g, 0.158 mmol) in acetone (3 mL). The clear solution was concentrated to ~ 1 mL and ethanol (10 mL) was added, resulting in the precipitation of TBA·BPh$_4$, which was removed by filtration. Diethyl ether (20 mL) was added to the filtrate causing the formation of a precipitate. This was isolated by filtration and washed with ethanol/diethyl ether (1:2 v/v, 2 × 5 mL) to give **2·4Br** as an off-white powder. Yield: 0.108 g (0.126 mmol, 79%).

^{1}H NMR (d$_6$-DMSO): δ 9.30 (br. s, 8H), 8.97 (br. s, 8H), 7.86 (d, *J* = 8.3 Hz, 8H), 7.56 (d, *J* = 8.3 Hz, 8H) ppm.

LRESI-MS (pos.) 489.3, calc. for $[C_{29}H_{29}N_8]^+$ (*i.e.* loss of 3 H^+ and 4 Br^-) = 489.3;

245.2, calc. for $[C_{29}H_{30}N_8]^{2+}$ (*i.e.* loss of 2 H^+ and 4 Br^-) = 245.1 Da.

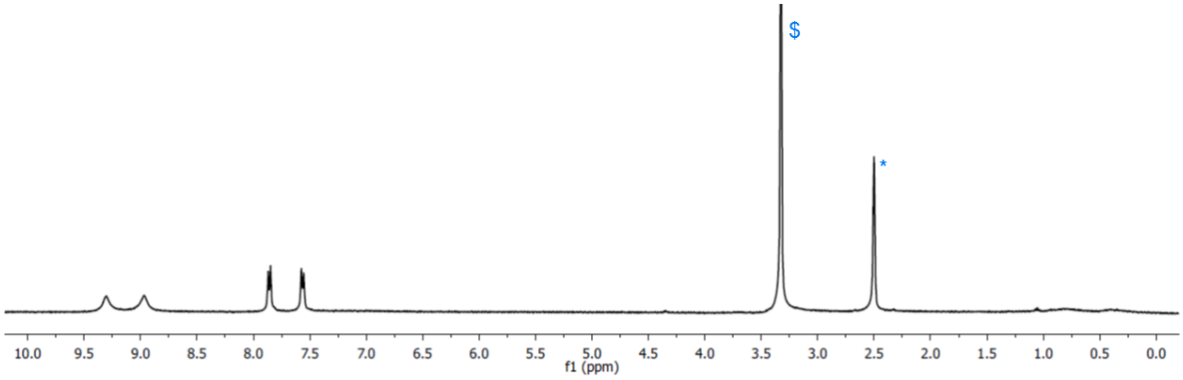

Figure S8. ^{1}H NMR spectrum of **2·4Br** (400 MHz, 298 K, d$_6$-DMSO, peak marked * corresponds to residual solvent signal, peak marked $ corresponds to water).

2·4NO$_3$

A solution of TBA·NO$_3$ (0.050 g, 0.16 mmol) in acetone (5 mL) was added to a solution of **2·4BPh$_4$** (0.050 g, 0.028 mmol) in acetone (3 mL). The clear solution was concentrated to ~ 1 mL and ethanol (10 mL) was added, resulting in the precipitation of TBA·BPh$_4$, which was removed by filtration. Diethyl ether (20 mL) was added to the filtrate causing the formation of a precipitate. This was isolated by filtration and washed with ethanol/diethyl ether (1:2 v/v, 2 × 5 mL) to give **2·4NO$_3$** as a white powder. Yield: 0.020 g (0.027 mmol, 95%).

^{1}H NMR (d$_6$-DMSO): δ 9.24 (br. s, 8H), 9.00 (br. s, 8H), 7.83 (d, *J* = 8.3 Hz, 8H), 7.56 (d, *J* = 8.3 Hz, 8H) ppm.

LRESI-MS (pos.) 489.3, calc. for $[C_{29}H_{29}N_8]^+$ (*i.e.* loss of 3 H^+ and 4 NO_3^-) = 489.3;

245.2, calc. for $[C_{29}H_{30}N_8]^{2+}$ (*i.e.* loss of 2 H^+ and 4 NO_3^-) = 245.1 Da.

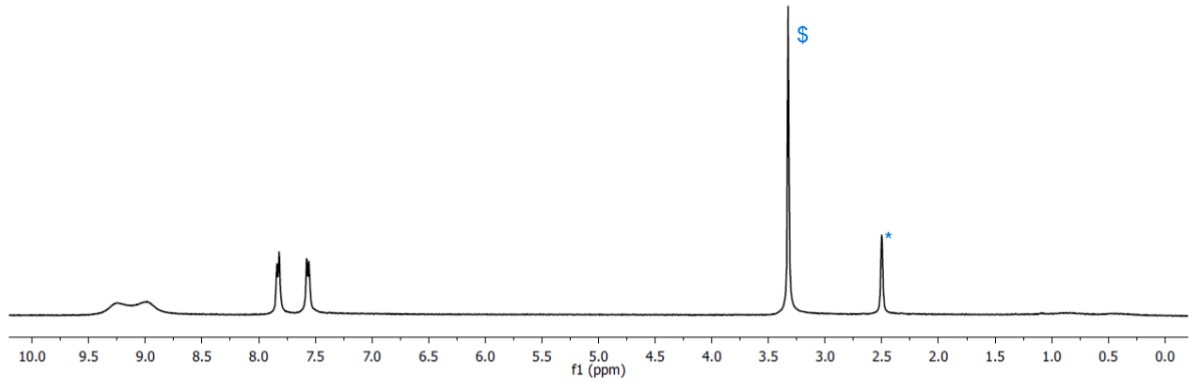

Figure S9. ^{1}H NMR spectrum of **2·4NO$_3$** (400 MHz, 298 K, d$_6$-DMSO, peak marked * corresponds to residual solvent signal, peak marked $ corresponds to water).

Synthesis of tet-[2·(TP)$_2$]$_n$ and ortho-[2·(TP)$_2$]$_n$

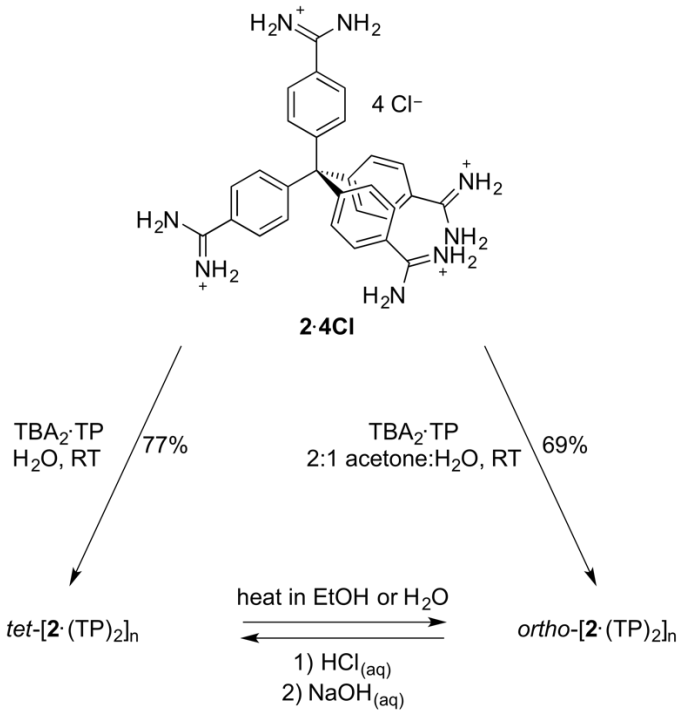

Scheme S3. Synthesis of *tet*-[**2**·(TP)$_2$]$_n$ and *ortho*-[**2**·(TP)$_2$]$_n$ and conversion between the two phases (TBA$_2$·TP = tetrabutylammonium terephthalate).

tet-[**2**·(TP)$_2$]$_n$

The synthesis of *tet*-[**2**·(TP)$_2$]$_n$ is described in the main article.

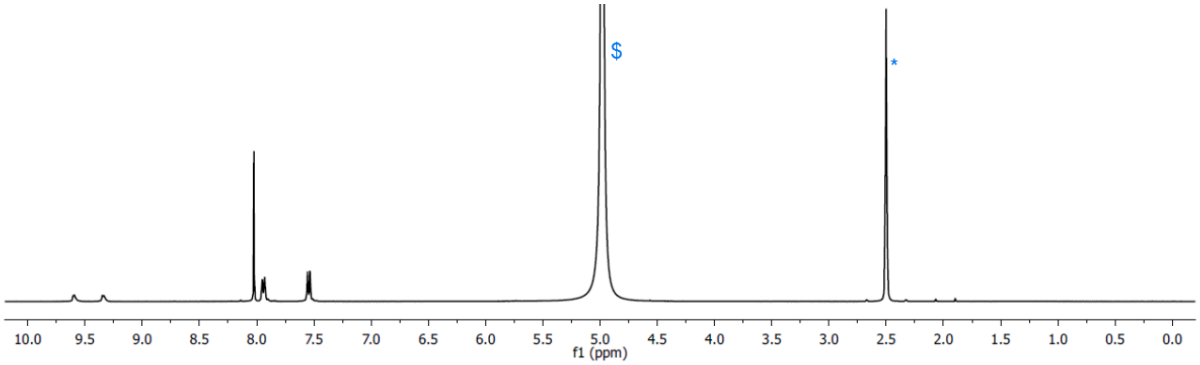

Figure S10. ^{1}H NMR spectrum of *tet*-[**2**·(TP)$_2$]$_n$ after acid digestion·(400 MHz, 298 K, d_6-DMSO containing a drop of conc. DCl$_{(aq)}$, peak marked * corresponds to residual solvent signal, peak marked $ corresponds to water).

Table S1. Raw data and calculated elemental analysis percentages for *tet*-[**2**·(TP)$_2$]$_n$.

***tet*-[2·(TP)$_2$]$_n$**	**C**	**H**	**N**
observed values, run 1	63.52	5.61	12.80
observed values, run 2	63.57	5.67	12.85
observed values, average	*63.55*	*5.64*	*12.83*
*calc. for [**2**·(TP)$_2$]·2H$_2$O*	*63.08*	*5.18*	*13.08*

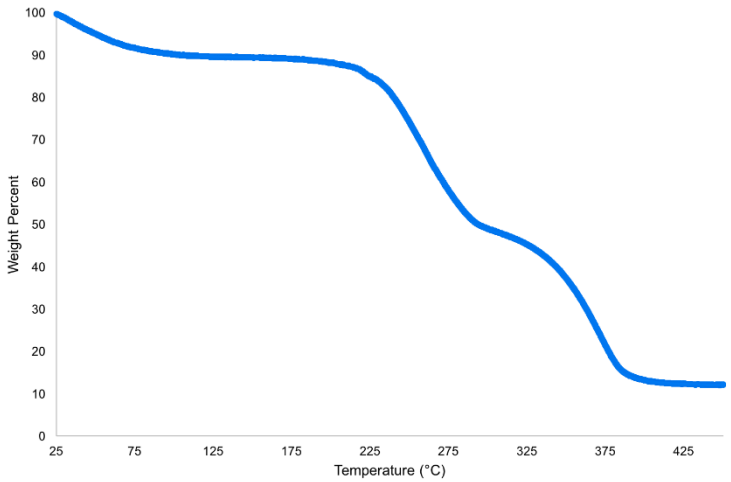

Figure S11. TGA trace of *tet*-[**2**·(TP)$_2$]$_n$.

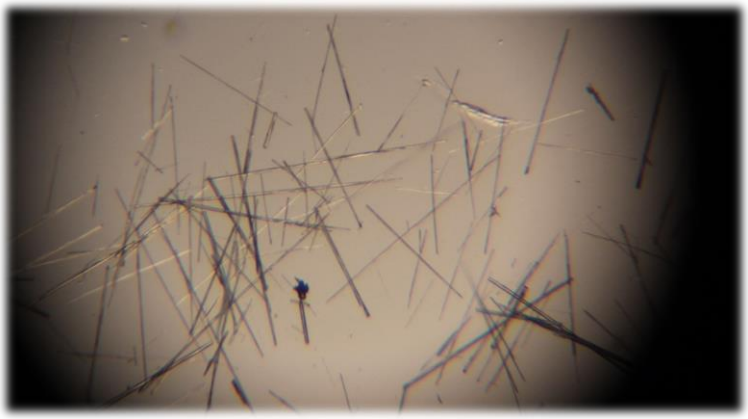

Figure S12. Photograph of needle-like crystals of *tet*-[**2**·$(TP)_2$]$_n$ taken through an optical microscope.

***ortho*-[2·(TP)$_2$]$_n$**

The synthesis of *ortho*-[**2**·(TP)$_2$]$_n$ is described in the main article.

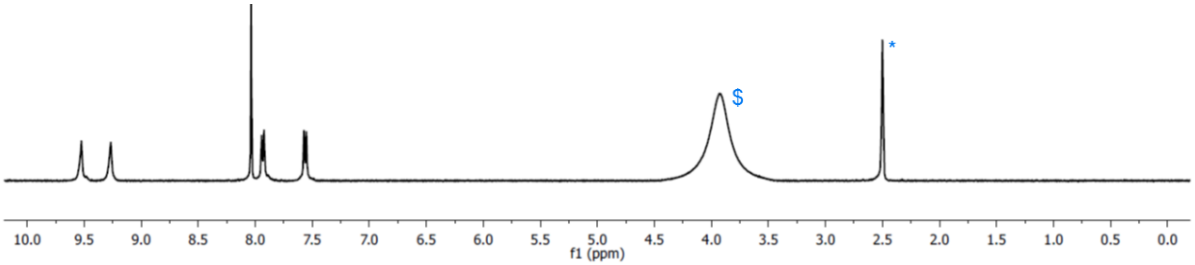

Figure S13. ^{1}H NMR spectrum of *ortho*-[**2**·(TP)$_2$]$_n$ after acid digestion·(400 MHz, 298 K, d_6-DMSO containing a drop of conc. DCl$_{(aq)}$, peak marked * corresponds to residual solvent signal, peak marked $ corresponds to water).

Table S2. Raw data and calculated elemental analysis percentages for *ortho*-[**2**·(TP)$_2$]$_n$.

***ortho*-[2·(TP)$_2$]$_n$**	**C**	**H**	**N**
observed values, run 1	60.94	5.65	12.16
observed values, run 2	61.01	5.72	12.16
observed values, average	*60.98*	*5.69*	*12.16*
*calc. for [**2**·(TP)$_2$]·4H$_2$O*	*60.53*	*5.42*	*12.55*

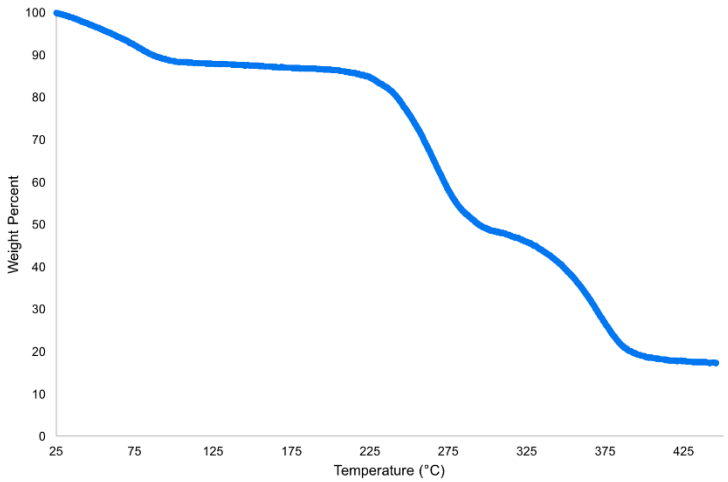

Figure S14. TGA trace of *ortho*-[**2**·$(TP)_2$]$_n$.

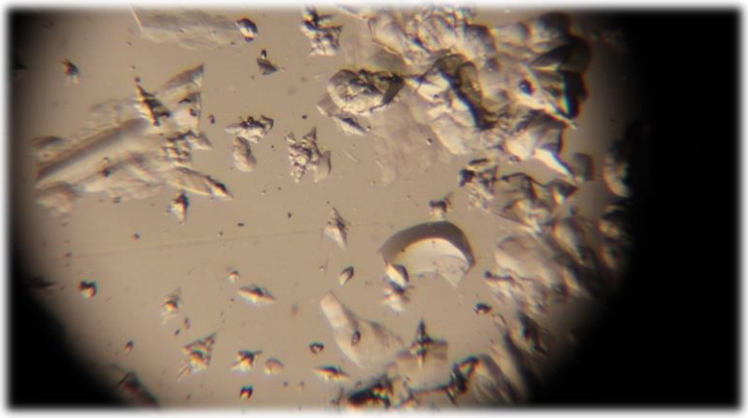

Figure S15. Photograph of plate-like crystals of *ortho*-[**2**·$(TP)_2$]$_n$ taken through an optical microscope.

The conditions shown in Scheme S3 are only some of the possible methods of preparing *tet*- and *ortho*-[**2**·$(TP)_2$]$_n$. Other methods are listed in Table S2.

Table S2. Conditions used to prepare [**2**·$(TP)_2$]$_n$ and structure of the framework product (all solvent ratios are volume:volume ratios).

Conditions	Product
Varying starting materials in water	
2·4Cl and TBA_2·TP	*tet*-[**2**·$(TP)_2$]$_n$
2·4Cl and sodium terephthalate	*tet*-[**2**·$(TP)_2$]$_n$
2·4Br and TBA_2·TP	*tet*-[**2**·$(TP)_2$]$_n$
2·4NO_3 and TBA_2·TP	*tet*-[**2**·$(TP)_2$]$_n$
***2·4Cl** and TBA_2·TP in water/acetone*	
100% water	*tet*-[**2**·$(TP)_2$]$_n$
90:10 water:acetone	*ortho*-[**2**·$(TP)_2$]$_n$
80:20 water:acetone	*ortho*-[**2**·$(TP)_2$]$_n$
70:30 water:acetone	*ortho*-[**2**·$(TP)_2$]$_n$
60:40 water:acetone	*ortho*-[**2**·$(TP)_2$]$_n$
50:50 water:acetone	*triclinic*-[**2**·$(TP)_2$]$_n$*
***2·4Cl** and TBA_2·TP in water/ethanol*	
100% water	*tet*-[**2**·$(TP)_2$]$_n$
98:2 water:ethanol	*ortho*-[**2**·$(TP)_2$]$_n$
99:1 water:ethanol	*ortho*-[**2**·$(TP)_2$]$_n$
***2·4Cl** and TBA_2·TP in $NaCl_{(aq)}$*	
0 mM $NaCl_{(aq)}$	*tet*-[**2**·$(TP)_2$]$_n$
10 mM $NaCl_{(aq)}$	*tet*-[**2**·$(TP)_2$]$_n$
50 mM $NaCl_{(aq)}$	*tet*-[**2**·$(TP)_2$]$_n$
100 mM $NaCl_{(aq)}$	mixture of *tet*-[**2**·$(TP)_2$]$_n$ and *ortho*-[**2**·$(TP)_2$]$_n$, major product is *ortho*-[**2**·$(TP)_2$]$_n$
Other	
1:2:2 **2·4Cl**:TBA_2·TP:TBA_2·SO_4 (*i.e.* one equivalent of sulfate per terephthalate anion)	*ortho*-[**2**·$(TP)_2$]$_n$

* This gives a new phase of the product with a triclinic space group, see the CIF for more details.

Framework switching and disassembly/re-assembly

Conversion of ortho-[2·(TP)$_2$]$_n$ to tet-[2·(TP)$_2$]$_n$

Freshly-prepared *tet*-[**2**·(TP)$_2$]$_n$ (~0.020 g) was removed from the crystallisation liquor, suspended in water (1 mL) and heated at 70 °C for 2 hours. It was cooled to room temperature, and the crystals washed with water and dried. Yield: 0.016 g (~80%).

An identical procedure but using ethanol (1 mL) instead of water gave identical results.

Characterisation data for material prepared in this way were the same as for *ortho*-[**2**·(TP)$_2$]$_n$ prepared by other methods, except that the crystals had a needle morphology, similar to the *tetragonal* crystals that they were prepared from, with additional "bumps" on the side (Figure S16).

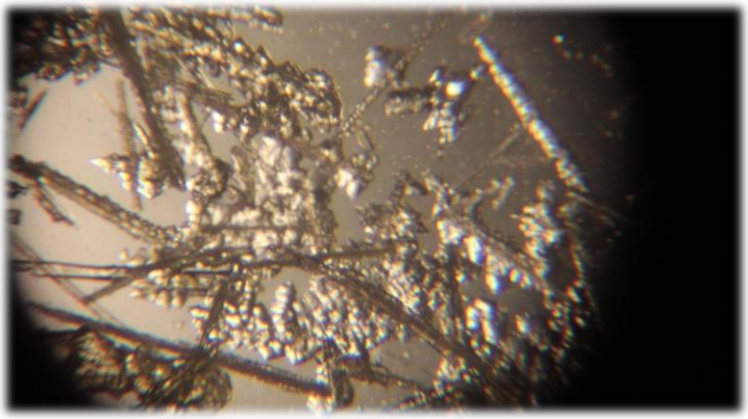

Figure S16. Photograph of needle-like crystals of *ortho*-[**2**·(TP)$_2$]$_n$ prepared by heating *tet*-[**2**·(TP)$_2$]$_n$ in water. Photographs taken through an optical microscope.

Conversion of tet-[2·(TP)$_2$]$_n$ to ortho-[2·(TP)$_2$]$_n$, and framework disassembly and re-assembly

Ortho-[**2**·(TP)$_2$]$_n$ (0.010 g, 0.012 mmol) was suspended in HCl$_{(aq)}$ (0.1 M, 1 mL) and sonicated for 15 minutes causing all crystals to disappear and a white powder to form (terephthalic acid). NaOH$_{(aq)}$ (0.1 M, ~ 1 mL) was added until very slightly basic (pH ~ 8), by which point all material had dissolved to give a clear colourless solution. Within 10 minutes needle-like crystals formed, and crystallisation was complete within 1 hour. These crystals were collected, washed with water and air-dried, giving *tet*-[**2**·(TP)$_2$]$_n$. Isolated yield: 0.007 g (0.008 mmol, ~70%).

The product identity and phase purity were confirmed by SCXRD and PXRD.

*Starting from tet-[**2**·(TP)$_2$]$_n$ gave identical results.*

Powder X-ray diffraction (PXRD)

General comments on PXRD

PXRD data were recorded at room temperature on a PANalytical Empyrean diffractometer using Cu Kα radiation and a PIXcel detector.

PXRD of tet-[2·(TP)$_2$]$_n$

As shown in Figure S17, after removal from solvent, *tet*-[**2**·(TP)$_2$]$_n$ initially shows negligible crystallinity by PXRD. Over time, the structure becomes more crystalline before subsequently losing this crystallinity. The observed PXRD pattern after 60 minutes is consistent with that calculated from the SCXRD data (albeit with some peaks not observed); the slight offset in peak positions occurs due to the different temperatures at which the SCXRD and PXRD data were recorded (150 and 293 K, respectively).

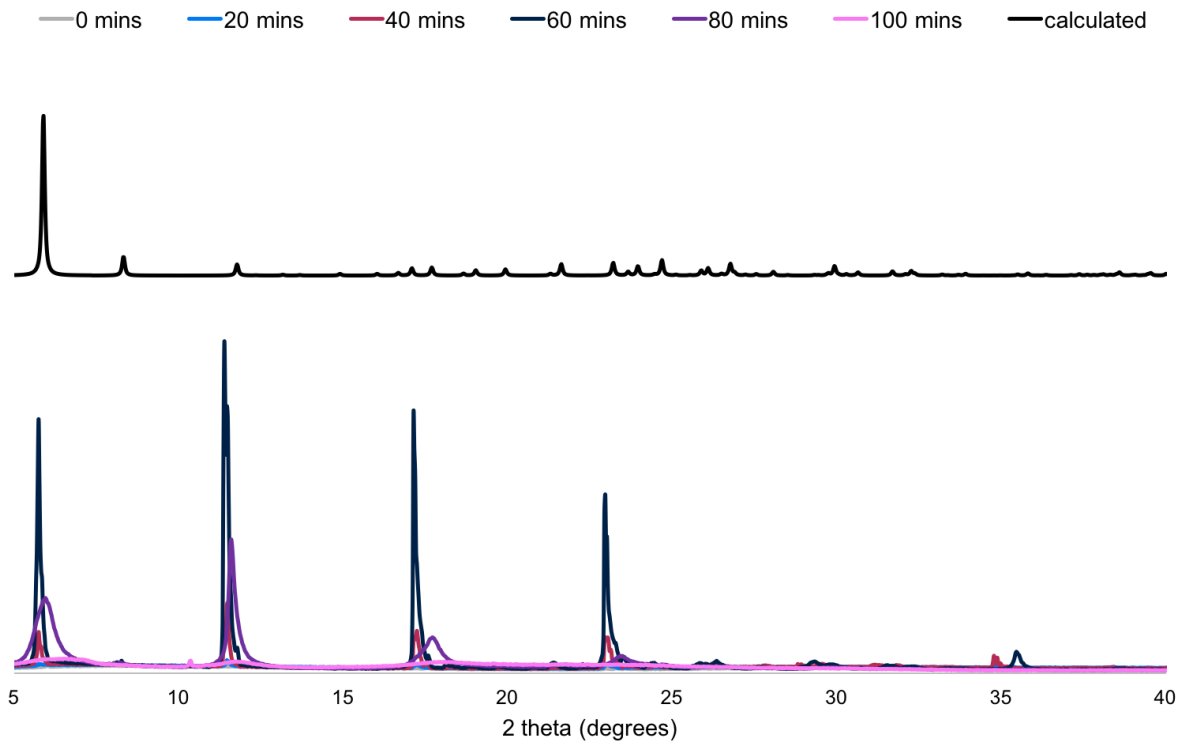

Figure S17. PXRD traces of *tet*-[**2**·(TP)$_2$]$_n$ over time, and comparison with PXRD pattern calculated from SCXRD data. The time given is the approximate amount of time between the sample being removed from solvent and the PXRD data being recorded.

Rehydration of tet-[2·(TP)$_2$]$_n$

Once *tet*-[**2**·(TP)$_2$]$_n$ had dried completely and was acrystalline (~ 2 hours), its crystallinity could be restored by adding a drop of water to the sample (Figure S18). It takes a short time for the crystallinity to redevelop, and if the water is allowed to evaporate, crystallinity is again lost over a period of approximately an hour.

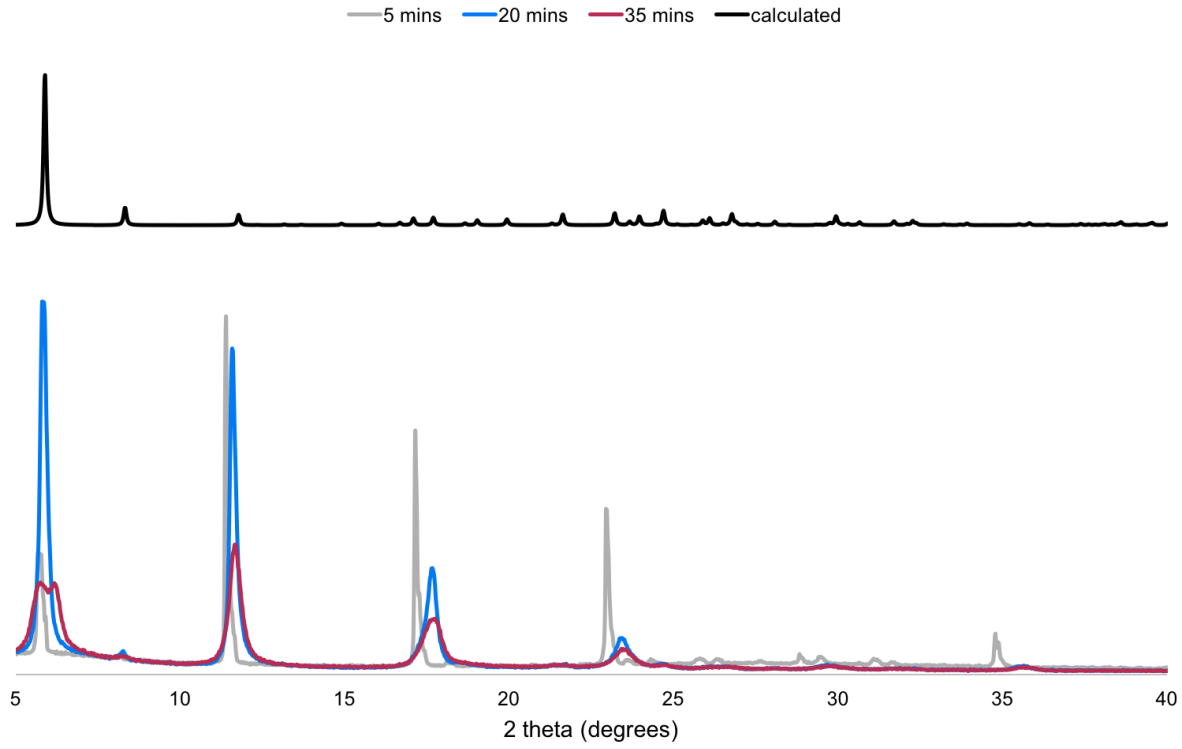

Figure S18. PXRD traces of a sample of *tet*-[**2**·(TP)$_2$]$_n$ that has become acrystalline due to "drying out," and its "recovery" over time upon addition of a drop of water. A comparison with the PXRD pattern calculated from SCXRD data is also provided. The time given is the approximate amount of time between the drop of water being added, and the PXRD data being recorded.

PXRD of ortho-[2·(TP)$_2$]$_n$

Ortho-[**2**·(TP)$_2$]$_n$ was isolated, thoroughly dried *in vacuo* and PXRD data recorded (Figure S19, 0 days). The same sample was then kept in a vial on the benchtop for four weeks, and then PXRD recorded again (Figure S19, 4 weeks). No significant changes in the PXRD patterns were observed, suggesting a relatively robust material. Good agreement is observed between the observed patterns and that calculated from the SCXRD data (Figure S19, calculated); the slight offset in peak positions occurs due to the different temperatures at which the SCXRD and PXRD data were recorded (150 and 293 K, respectively).

PXRD patterns of *ortho*-[**2**·(TP)$_2$]$_n$ prepared from water containing organic co-solvents were the same as those for *ortho*-[**2**·(TP)$_2$]$_n$ prepared by boiling *tet*-[**2**·(TP)$_2$]$_n$.

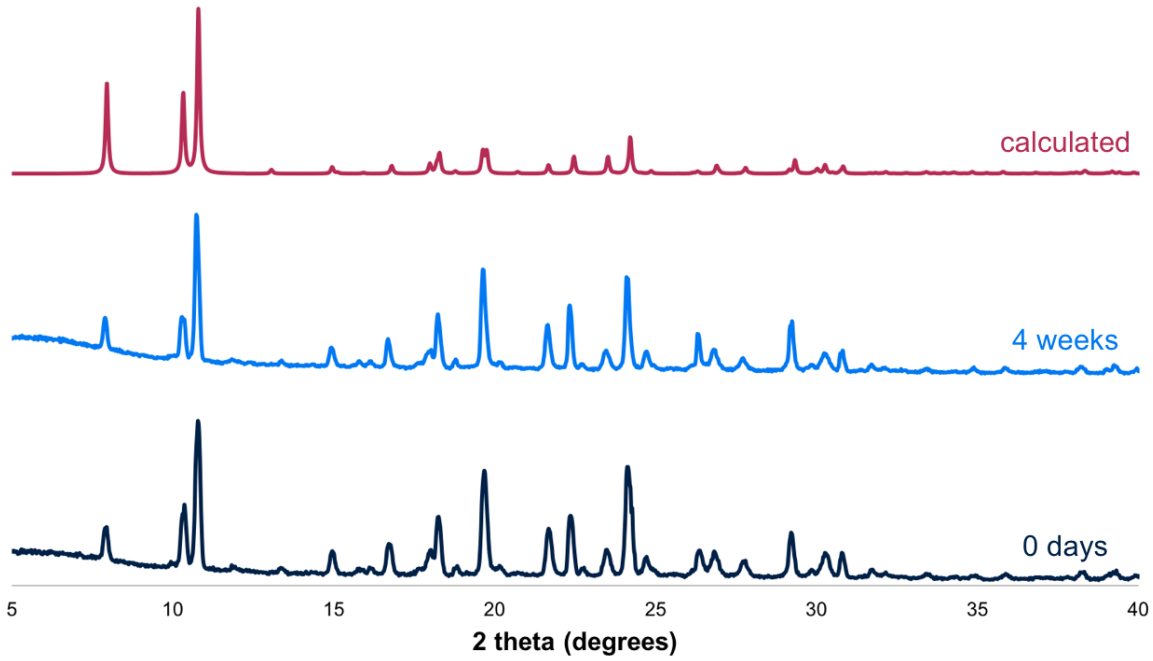

Figure S19. PXRD traces of vacuum-dried *ortho*-[**2**·(TP)$_2$]$_n$ zero days and four weeks after isolation, and comparison with PXRD pattern calculated from SCXRD data..

Conversion of tet-[2·(TP)$_2$]$_n$ to ortho-[2·(TP)$_2$]$_n$

Once *tet*-[**2**·(TP)$_2$]$_n$ had dried completely and was acrystalline (~ 2 hours), it could be converted to *ortho*-[**2**·(TP)$_2$]$_n$ by addition of ethanol (Figure S20). It takes a short time for the crystallinity to redevelop, and ethanol must be added approximately every 20 minutes to replace solvent lost to evaporation. If crystals of dried *tet*-[**2**·(TP)$_2$]$_n$ are submerged in ethanol for 2 hours, complete conversion to *ortho*-[**2**·(TP)$_2$]$_n$ is observed, and once complete conversion is achieved, the structure remains crystalline after drying *in vacuo*.

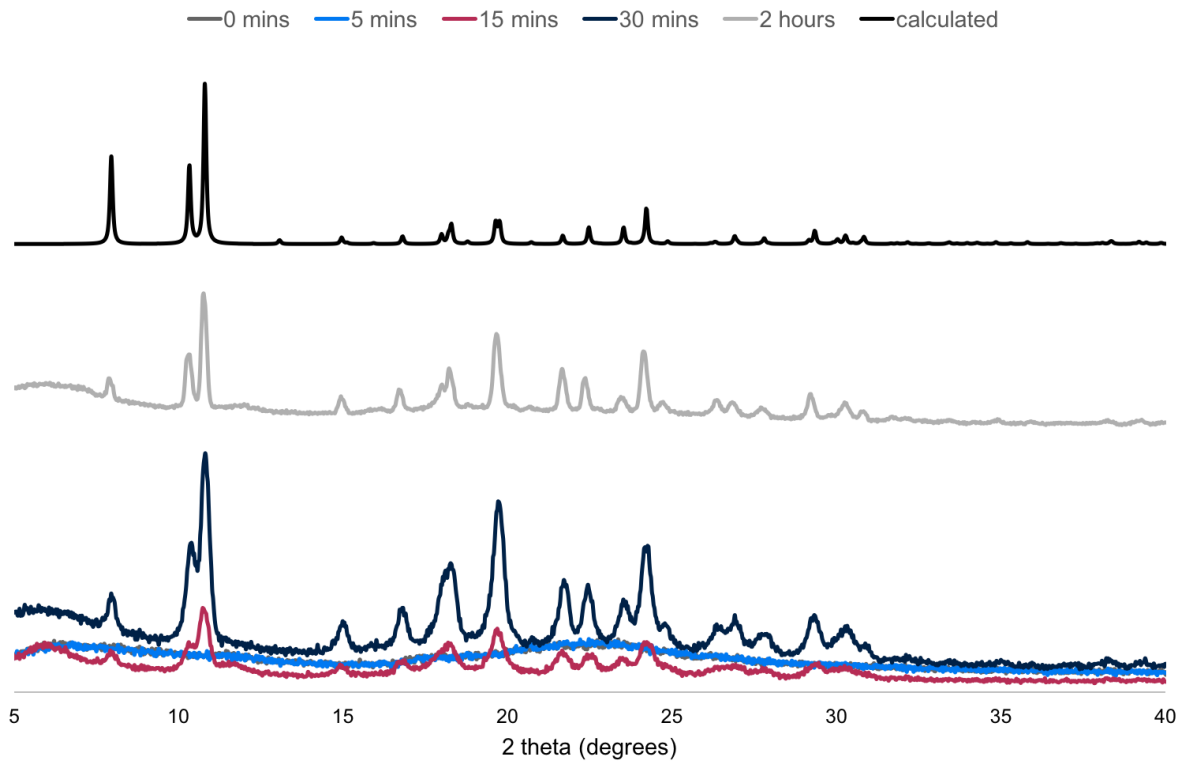

Figure S20. PXRD traces of a sample of *tet*-[**2**·(TP)$_2$]$_n$ that has become acrystalline due to "drying out," and its conversion to *tet*-[**2**·(TP)$_2$]$_n$ over time upon addition of drops of ethanol (0 minutes to 30 minutes). The time given is the approximate amount of time between the first drop of ethanol being added, and the PXRD data being recorded. The 2 hour PXRD trace was a separate sample of the same dehydrated framework that was submerged in ethanol for 2 hours. A comparison with the PXRD pattern calculated from SCXRD data for *ortho*-[**2**·(TP)$_2$]$_n$ is also provided.

Single crystal X-ray diffraction (SCXRD)

General comments on SCXRD

Data were collected using mirror-monochromated Cu Kα radiation on an Agilent SuperNova diffractometer. Crystals were cooled to 150 K using a Cryostream N2 open-flow cooling device[S6] in all cases. Raw frame data (including data reduction, interframe scaling, unit cell refinement and absorption corrections) were processed using CrysAlisPro.[S7]

Structures were solved with SUPERFLIP[S8] and refined using full-matrix least-squares on F^2 within the CRYSTALS suite.[S9] All non-hydrogen atoms were refined with anisotropic displacement parameters. C–H hydrogen atoms were generally visible in the Fourier difference map, and were initially refined with restraints on bond lengths and angles, after which the positions were used as the basis for a riding model.[S10] O–H and N–H hydrogen atoms were generally visible in the Fourier difference map and were refined with restraints on bond lengths and angles.

Full crystallographic data in CIF format are provided as Supporting Information (CCDC Numbers: 1523337–1523341). Selected data are summarised in Table S3 and individual structures are discussed in more detail below.

Structure of 1·BzO

Crystals were obtained by carefully layering an acetonitrile solution of **1·BPh$_4$** with an acetonitrile solution of TBA·BzO; crystals formed within a day. Crystals could also be obtained in the same manner using 95:5 acetonitrile:water instead of acetonitrile; a dataset collected from these gave a structure that was indistinguishable from that collected from crystals grown from acetonitrile.

All crystals appeared to be split (lengthwise down the long dimension of the lath-like crystals). Several crystals were examined, but all gave “split”-looking diffraction patterns. Analysis using ROTAX[S11] indicated the presence of two twin components, and an appropriate twin law was inserted within CRYSTALS[S9], and the occupancy of the two components refined.

Apart from restraints on N–H bond lengths and angles, it was not necessary to use any crystallographic restraints.

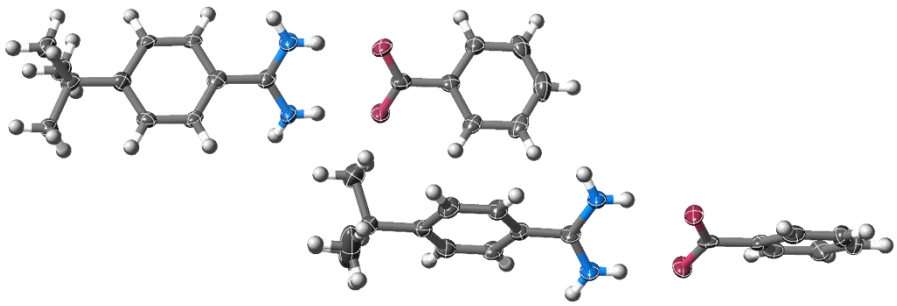

Figure S21. Thermal ellipsoid plot of the asymmetric unit cell of **1·BzO** (ellipsoids shown at 50% probability level).

Structure of tet-[2·(TP)$_2$]·18.8H$_2$O

Twinned crystals were obtained by mixing aqueous solutions of **2·4Cl** and TBA$_2$·TP. A total of five datasets were collected from different batches of crystals – in all cases, twinned crystals were obtained, with essentially identical structures (including the number and approximate occupancy of water solvent molecules). An appropriate twin law was found using the ROTAX[S11] package within CRYSTALS.[S9] The occupancies of the two twin components were refined.

The asymmetric unit cell contains one quarter of a molecule of **2**$^{4+}$, one half of a terephthalate anion and a total of 4.7 water molecules (comprised of three full-occupancy, two 0.6-occupancy and one half-occupancy water).

Hydrogen atoms on water molecules were not clearly visible in the Fourier difference map, and it was not possible to sensibly refine the positions of these hydrogen atoms: therefore these atoms were inserted at idealised hydrogen bonding positions with O–H distances of 0.85 Å and ride on their attached oxygen atoms. Apart from restraints on N–H bond lengths and angles, it was not necessary to use any crystallographic restraints.

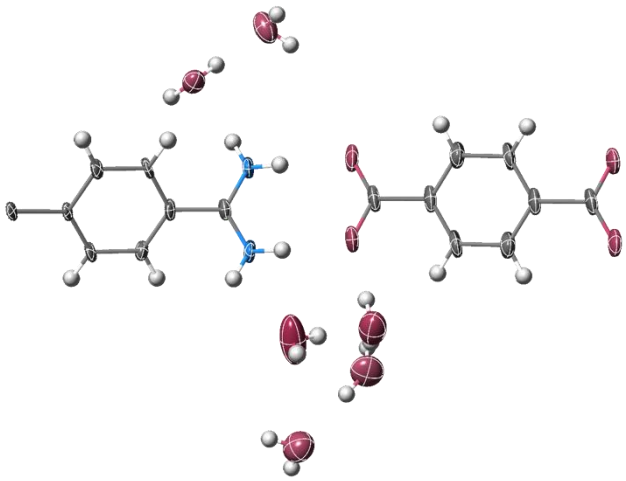

Figure S22. Thermal ellipsoid plot of the asymmetric unit cell of *tet*-[**2**·(TP)$_2$]·18.8H$_2$O (ellipsoids shown at 50% probability level).

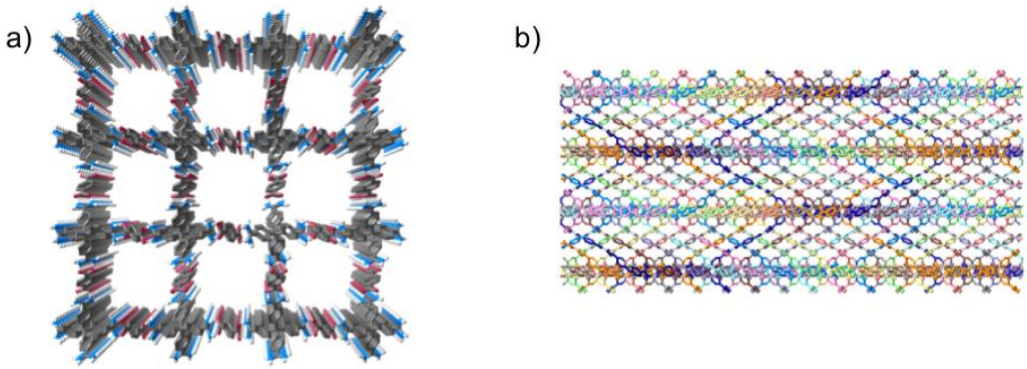

Figure S23. Additional views of the packing of *tet*-[**2**·(TP)$_2$]$_n$: a) view along the *c*-axis; b) view along the *a*/*b*-axis showing the 11 interpenetrated nets (solvent molecules and some hydrogen atoms removed for clarity in both images).

Structure of ortho-[2·(TP)$_2$]·3H$_2$O

Single crystals were obtained by mixing solutions of **2·4Cl** and TBA$_2$·TP in 2:1 water:acetone and leaving the mixture to stand. A total of four datasets were collected on different batches of crystals. All showed essentially identical structures, including having the same number of water molecules, and the same two positions of the terephthalate anion.

The asymmetric unit cell contains one quarter of a molecule of $\mathbf{2}^{4+}$, half of a terephthalate anion (which is disordered over two positions) and two partial occupancy water molecules (one with occupancy of 0.5, and one with occupancy 0.25). Given that a large proportion of the structure is ill-defined (due to the terephthalate disorder and partial occupancy solvent molecules), it was found that all four datasets were of relatively low quality.

A superior refinement of the data could be obtained by using PLATON-SQUEEZE[S12] to account for the water molecules. If PLATON-SQUEEZE was used, then the only restraints needed in the final refinement were on thermal and vibrational ellipsoid parameters of the terephthalate anion, and on the N–H bond lengths and angles. If PLATON-SQUEEZE was not used, it was necessary to restrain all thermal and vibrational and ellipsoid parameters, as well as bond lengths and angles of the terephthalate anion and N–H bond lengths and angles. It was not possible to sensibly refine the hydrogen atom positions of the water molecules, and so these were inserted at idealised hydrogen bonding positions with O–H bond lengths of 0.85 Å and ride on the attached oxygen atoms.

For completeness, both refinements of the data (using PLATON-SQUEEZE and not using PLATON-SQUEEZE) are included in the Supporting Information and CIF.

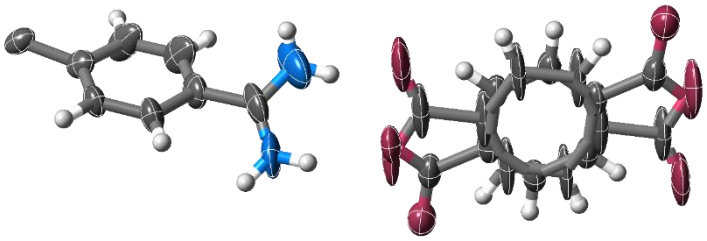

Figure S24. Thermal ellipsoid plot of the asymmetric unit cell of *ortho*-[**2**·(TP)$_2$]·3H$_2$O (ellipsoids shown at 50% probability level, PLATON-SQUEEZE[S12] used in refinement).

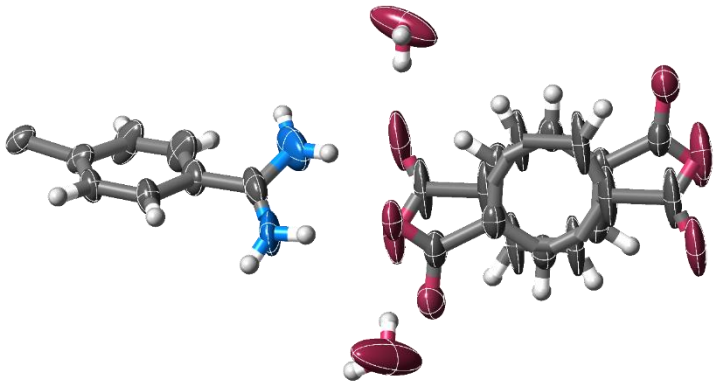

Figure S25. Thermal ellipsoid plot of the asymmetric unit cell of *ortho*-[**2**·$(TP)_2$]·$3H_2O$ (ellipsoids shown at 50% probability level, PLATON-SQUEEZE[S12] not used in refinement).

Table S3. Selected crystallographic data.

Compound	**1·BzO**	***tet*-[2·$(TP)_2$]·$18.8H_2O$**	***ortho*-[2·$(TP)_2$] PLATON-SQUEEZE used**	***ortho*-[2·$(TP)_2$]·$3H_2O$ PLATON-SQUEEZE not used**
Formula	$C_{11}H_{17}N_2$, $C_7H_5O_2$	0.25($C_{29}H_{32}N_8$), 0.5($C_8H_8O_4$), 4.7(H_2O)	0.25($C_{29}H_{32}N_8$), 0.5($C_8H_8O_4$)	0.25($C_{29}H_{32}N_8$), 0.5($C_8H_8O_4$), 0.75(H_2O)
Formula weight	298.39	289.88	205.22	218.73
a (Å)	9.9217(6)	30.0714(3)	14.7538(4)	14.7538(4)
b (Å)	10.0318(5)	30.0714(3)	19.4911(5)	19.4911(5)
c (Å)	18.7148(11)	7.38182(9)	34.2841(11)	34.2841(11)
α (º)	90.632(5)	90	90	90
β (º)	93.900(5)	90	90	90
γ (º)	119.479(6)	90	90	90
Unit cell volume (Å^3)	1615.70(9)	6675.29(8)	9859.0(4)	9859.0(4)
Crystal system	triclinic	tetragonal	orthorhombic	orthorhombic
Space group	$P\bar{1}$	$I4_1/a$	*Fddd*	*Fddd*
Z	4	16	32	32
Reflections (all)	12187	21972	34347	34347
Reflections (unique)	6328	2972	2212	2212
R_{int}	0.027	0.043	0.039	0.039
R_1 [$I > 2\sigma(I)$]	0.103	0.071	0.083	0.114
$wR_2(F^2)$ (all data)	0.284	0.200	0.217	0.319

Solution anion binding

Discussion of solution anion binding

Initial anion binding studies were conducted using ^{1}H NMR titration experiments in CD_3CN. While these revealed that **1·BPh$_4$** shows very strong binding of chloride anion in this solvent ($K_a > 10^4$ M^{-1}, Figures S26 and S27), addition of oxoanions caused precipitation.

We next attempted to study anion binding by ^{1}H NMR experiments in more competitive solvents (d_6-DMSO or 95:5 CD_3CN). In aqueous acetonitrile, the N–H resonances are not observed, presumably due to H/D exchange, and the C–H resonances do not move significantly upon addition of chloride or benzoate anions. In d_6-DMSO, addition of benzoate causes rapid disappearance of the N–H resonances, precluding quantitative titration experiments; addition of chloride does not cause disappearance of the N–H resonances and we were able to model the binding of this anion [K_a = 51(2) M^{-1}, Figures S28 and S29].

Given our primary interest is in carboxylate binding to amidinium groups, we next studied the anion binding properties of **1·BPh$_4$** using isothermal calorimetry (ITC). Preliminary studies of benzoate binding in DMSO suggested multiple binding equilibria, so we conducted studies in 95:5 CH_3CN:H_2O. In this solvent, no significant chloride anion binding was observed, but strong binding of benzoate was evident (K_a = 2910 ± 330 M^{-1}, Figure S30, with this binding being entropically driven (ΔH = +8.34 ± 0.84 kJ mol^{-1}). Entropically driven binding of oxoanions by a *guanidinium* receptor has been previously reported.[S13]

It is relatively surprising that such a simple receptor exhibits such potent anion recognition in a competitive aqueous medium, and so we turned to ^{13}C NMR to corroborate the results from ITC. These studies were hampered by the fact that **1$^+$** precipitates from 95:5 CD_3CN:D_2O at concentrations much greater than 2 mM^{-1}, meaning that ^{13}C NMR experiments had to be run in very dilute solution resulting in very long collection times on a high field spectrometer (~ 7 hours per ^{13}C spectrum on a 700 MHz spectrometer). Nevertheless, we were able to obtain several data points for addition of TBA·BzO or TBA·Cl to **1·BPh$_4$**.

Significant changes in all four phenyl ring ^{13}C resonances, as well as the amidinium ^{13}C resonance were observed upon addition of benzoate, with the amidinium resonance and the carbon atom closest to this moving downfield, while all other peaks move upfield. These peaks showed significant movement after one equivalent of anion, with much smaller shifts after continuing anion addition, consistent with relatively strong binding (Figure S30). While the quality of these fits is obviously low given the small number of datapoints, we were able to fit the peak movements to a 1:1 binding isotherm using *fittingprogram*[S14], obtaining approximate association constants of 1300–1900 M^{-1}. Importantly, addition of chloride anion to **1·BPh$_4$** resulted in only very minor shifts in the ^{13}C NMR resonances, and these shifts were approximately linear with increasing anion equivalents (*i.e.* there was no evidence of receptor saturation).

Given that the K_a values from ^{13}C NMR titrations are necessarily inexact due to the small number of datapoints, and that the K_a values from ITC and ^{13}C NMR were obtained at different concentrations using different techniques, there is reasonable concordance between the values, and indeed the concordance of the values is comparable to that observed in previous studies utilising both NMR and ITC techniques.[S15]

To further probe the interactions between **1**$^+$ and benzoate anions in solution, the system was examined using molecular dynamics (MD) simulations. Due to computational limitations, it was necessary to run this simulation at a concentration of 20 mM, rather than the lower concentrations used in ITC and NMR experiments. Experiments were run in triplicate, and by the end of all three simulations, all benzoate anions and **1**$^+$ cations had formed hydrogen bonded pairs, consistent with strong binding. No evidence of "stacked" pairs was observed with each cation/anion pair assembling through hydrogen bonding alone.

Taken together, the NMR, ITC and MD results suggest a relatively strong interaction between **1**$^+$ and BzO^- in a competitive aqueous medium, driven by the favourable hydrogen bonding possible between the complementary hydrogen bonding motifs.

^{1}H NMR binding studies

General protocol: all anion binding titration experiments were conducted at 298 K. Initial sample volumes were 0.50 mL and concentrations were 2.0 mmol L^{-1} of host. Solutions (100 mmol L^{-1}) of anions as tetrabutylammonium salts were added in aliquots, the samples thoroughly shaken and spectra recorded at 0.1, 0.2, 0.3, 0.4, 0.5, 0.6, 0.7, 0.8, 0.9, 1.0, 1.2, 1.4, 1.6, 1.8, 2.0, 2.5, 3.0, 3.5, 4.0, 5.0, 7.0 and 10 equivalents of anion. WINEQNMR2[S16] and *fittingprogram*[S14] were used to fit 1:1 binding isotherms.

Chloride anion binding: strong binding of chloride anion was observed in CD_3CN (Figures S26 and S27). The downfield N–H resonance was followed as this peak moved the most during the titration, but binding was too strong to be quantified by ^{1}H NMR methods ($K_a > 10^4$ M^{-1}). In d_6-DMSO, binding was significantly less strong (Figures S28 and S29); the downfield N–H resonance was again followed. Analysis using WINEQNMR2[S16] gave an association constant of 51 M^{-1}, with an estimated standard error of 2 M^{-1}; analysis using *fittingprogram* gave an association constant of 44 M^{-1}, with an estimated asymptotic error at a 95% confidence interval level of 2 M^{-1}.[S14]

Oxoanion binding: addition of benzoate, terephthalate or sulfate anions to **1·BPh$_4$** in CD_3CN caused precipitation.

In d_6-DMSO, addition of these anions caused the N–H resonances to broaden and then disappear (with less than 0.5 equivalents of anion added), while the C–H protons showed negligible movement over the course of the titration experiments, which is perhaps unsurprising as the nearest C–H proton is five bonds away from the amidinium binding site. In 95:5 CD_3CN:D_2O, the N–H resonances were not visible (presumably due to H/D exchange), and the C–H protons again showed negligible movement over the course of titration experiments.

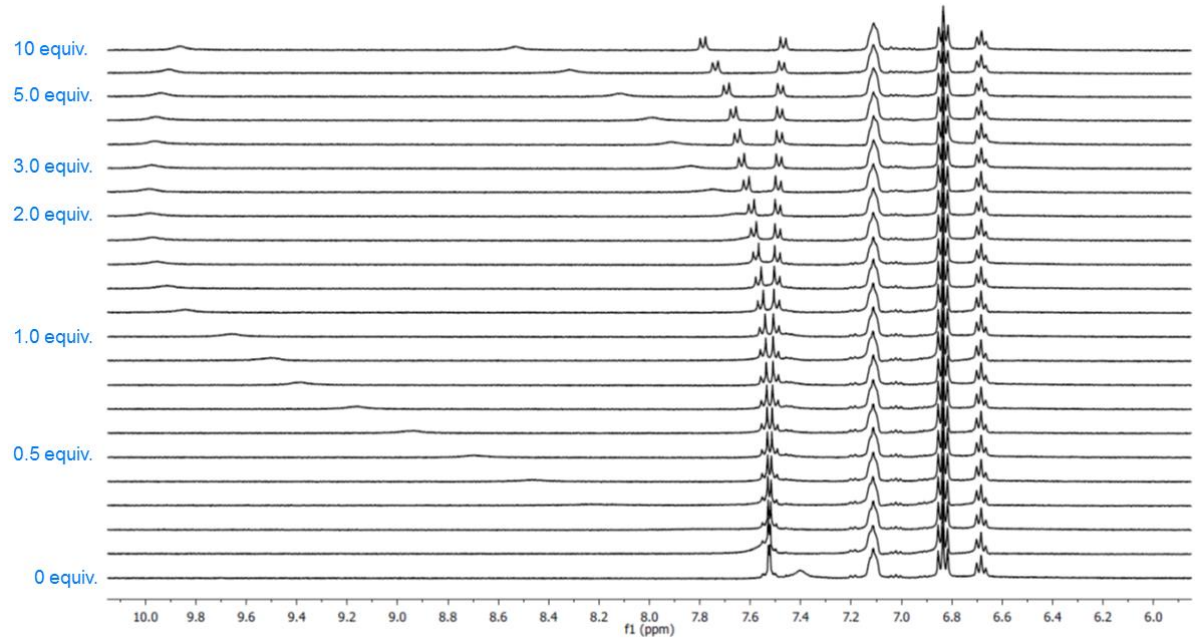

Figure S26. Partial ^{1}NMR spectra of **1·BPh$_4$** upon addition of TBA·Cl (400 MHz, 298 K, CD_3CN).

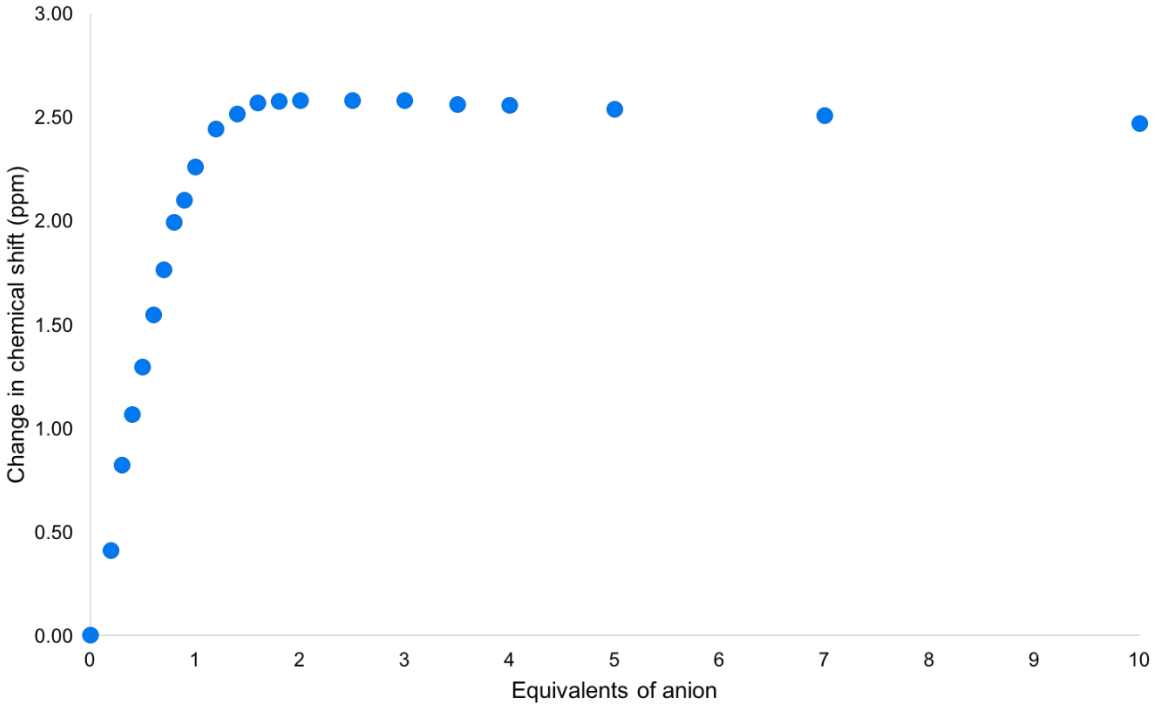

Figure S27. Change in chemical shift of downfield amidinium N–H proton upon addition of chloride anion (298 K, CD_3CN). Note: at 0.1 equivalents of anion, the N–H proton overlapped with other peaks and could not be adequately resolved, so this data point was not used when calculating the association constant.

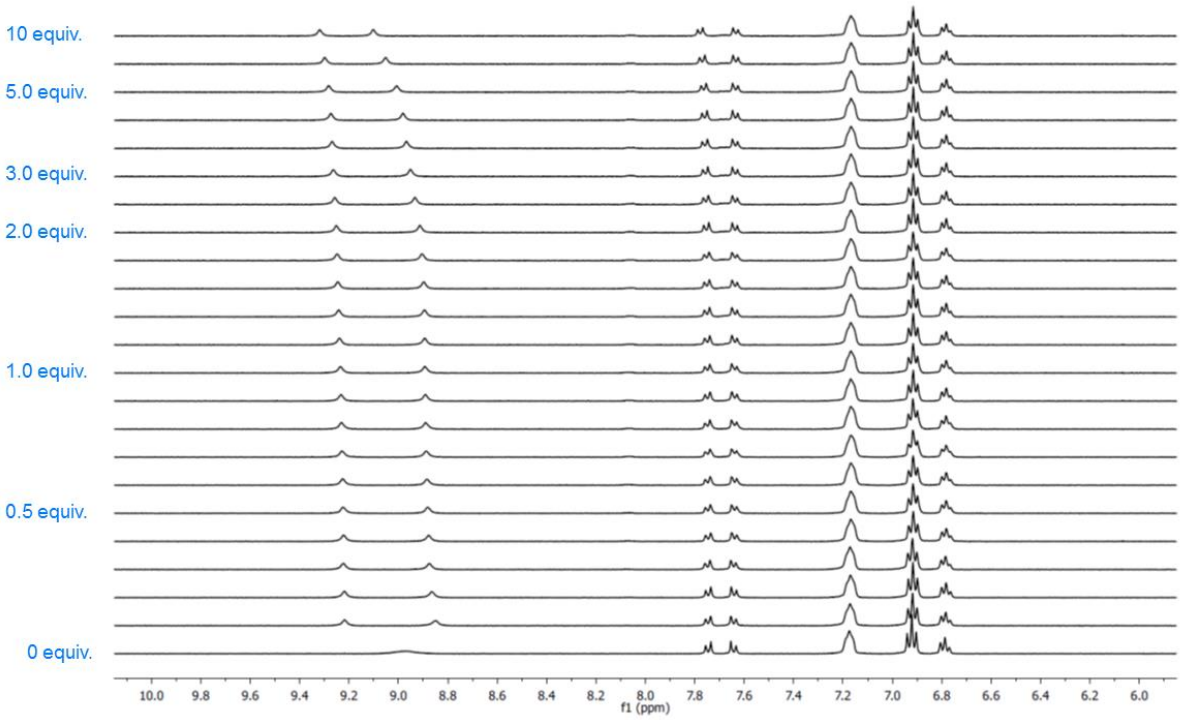

Figure S28. Partial ^{1}NMR spectra of **1·BPh$_4$** upon addition of TBA·Cl (400 MHz, 298 K, d_6-DMSO).

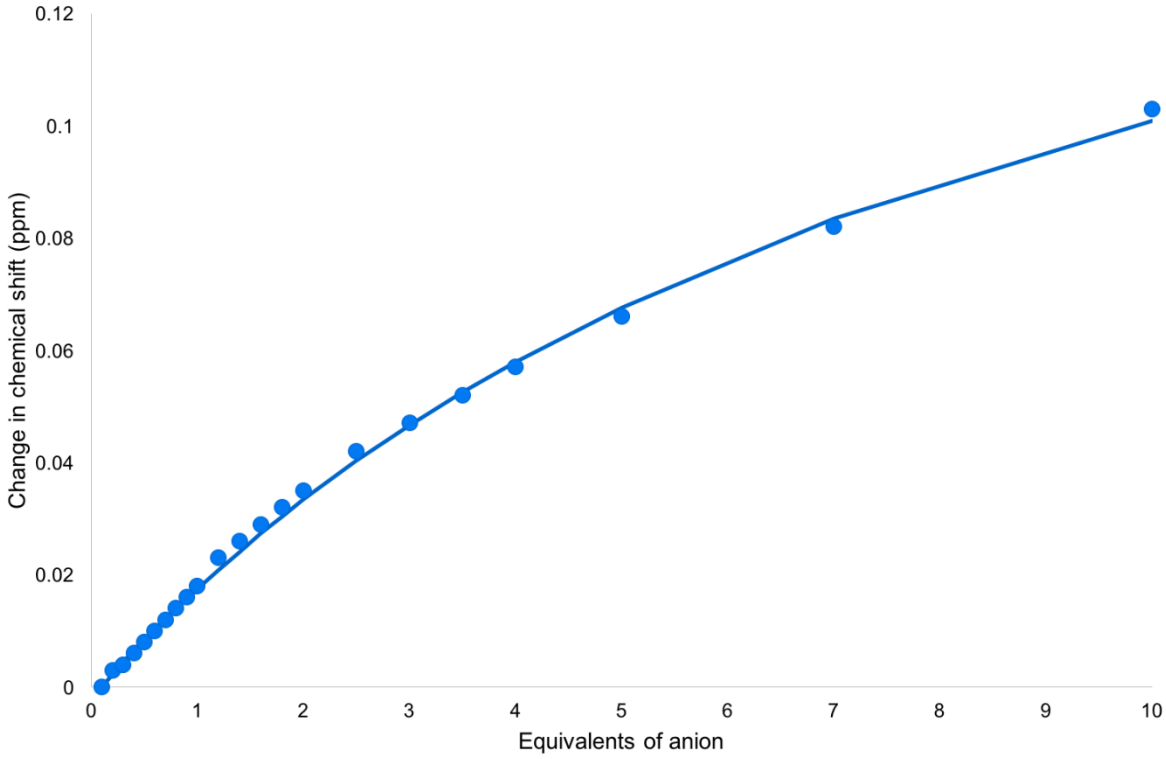

Figure S29. Experiment titration data (points) and fitted 1:1 binding isotherm from WINEQNMR2[S16] (line) for addition of TBA·Cl to **1·BPh$_4$** (298 K, d_6-DMSO). Note: at 0 equivalents of anion, the two N–H proton resonances overlapped, and so this data point was not used when calculating the association constant.

Isothermal calorimetry binding studies

General protocol: A Microcal VP-ITC calorimeter was used for all titrations. All titrations were conducted at 298 K. A total of 50 injections of 5 μL of a 50 mM^{-1} solution of TBA·Cl or TBA·BzO were added to a 1.0 mM^{-1} solution of **1·BPh₄** over 10 seconds, with a delay of 240 seconds between injections. A baseline was recorded by adding TBA·Cl or TBA·BzO solution into pure solvent and subtracting the blank solvent data from the titration data.

Binding in DMSO: Preliminary studies of the interaction between **1·BPh₄** and TBA·BzO in DMSO using ITC suggested multiple equilibria, and so no further studies were made in this solvent mixture.

Binding in 95:5 CH_3CN:H_2O: No evidence of binding between **1·BPh₄** and TBA·Cl was observed by ITC. Conversely, significant binding was observed upon addition of TBA·BzO to **1·BPh₄** (Figure S30).

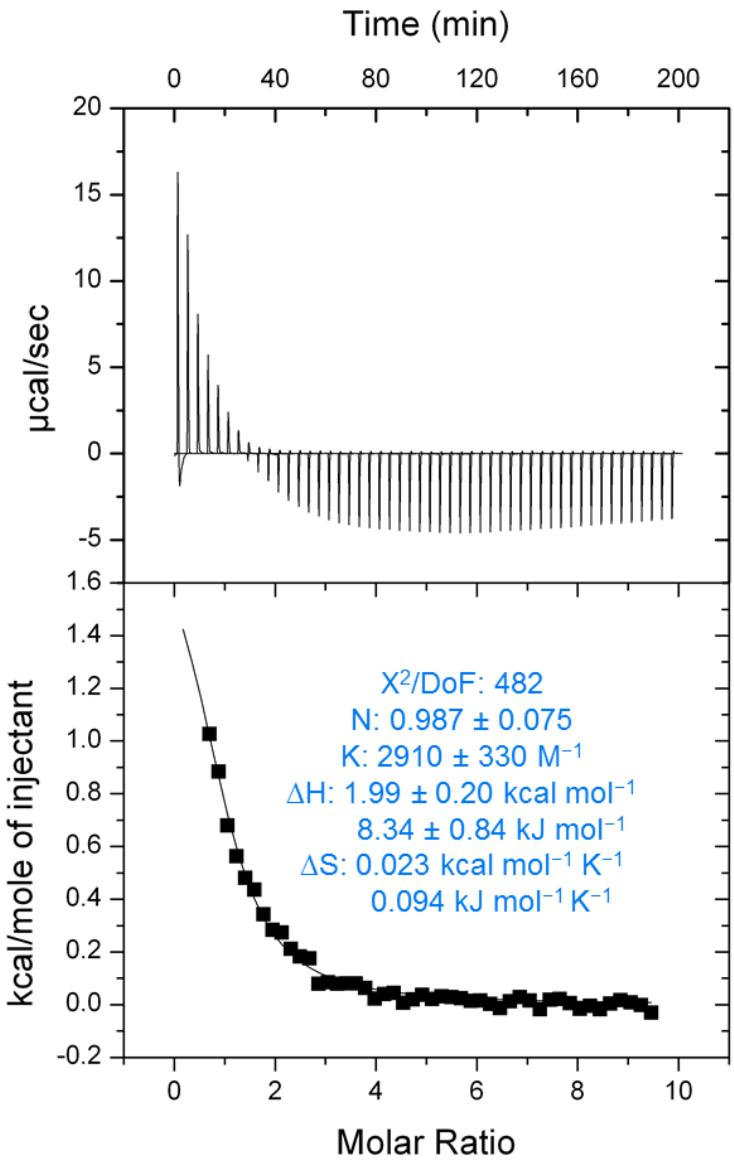

Figure S30. Experiment titration data (top graph, and points on bottom graph) and fitted 1:1 binding isotherm from (line on bottom graph) for addition of TBA·BzO to **1·BPh₄** (298 K. 95:5 CH_3CN:H_2O).

^{13}C NMR binding studies

General protocol: 2.0 mM solutions of **1·BPh$_4$** in 95:5 CD_3CN:D_2O were prepared containing either 0, 1, 2 or 5 equivalents TBA·BzO or 0, 1 or 5 equivalents of TBA·Cl. ^{1}H and ^{13}C NMR spectra of these solutions were recorded on a 700 MHz NMR (Figure S31). Due to the low concentrations of the solutions used, these required collecting large numbers of scans, and gave spectra with relatively poor signal-to-noise. Nevertheless, the peak positions could be located, and information about binding inferred.

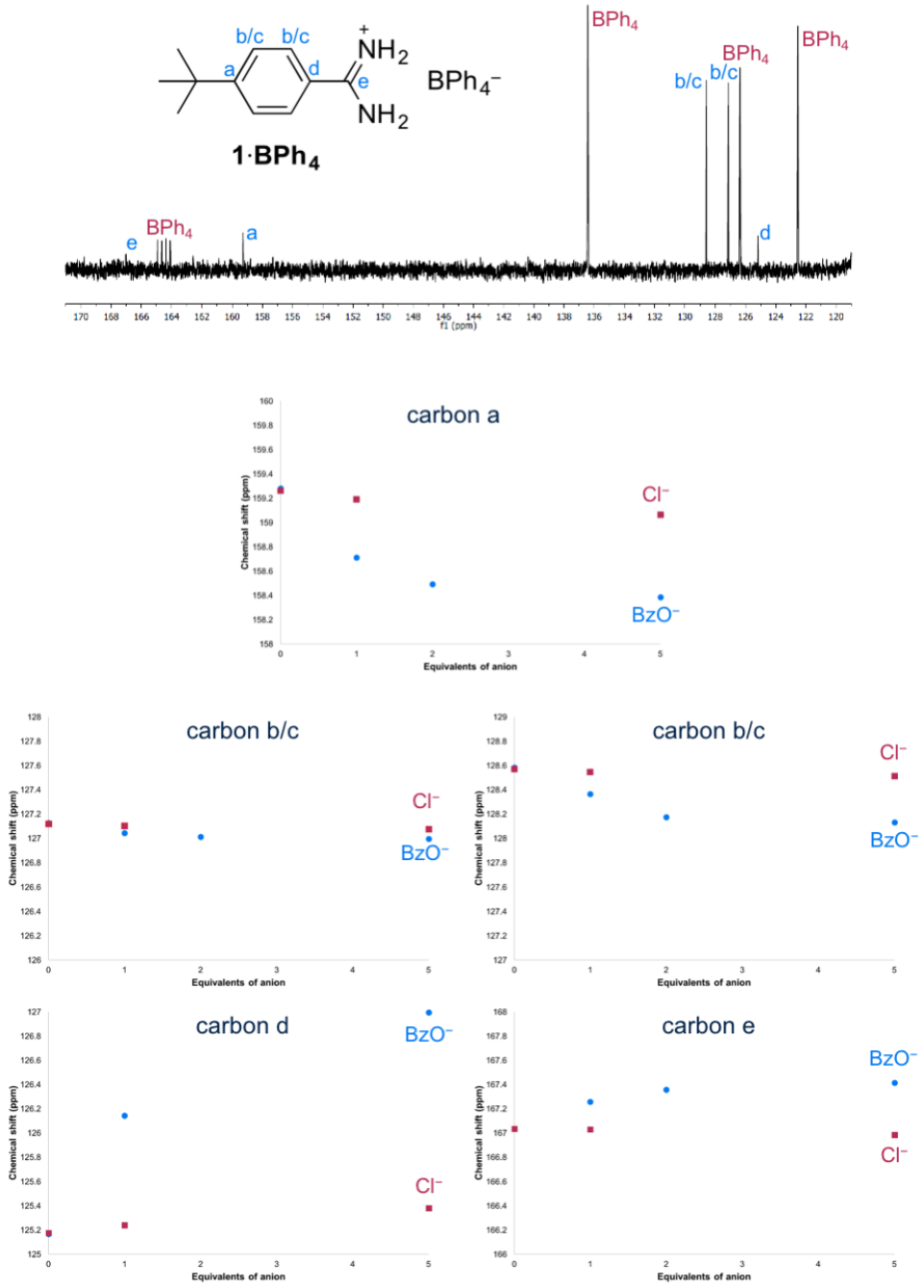

Figure S31. Assigned partial ^{13}C NMR spectrum of **1·BPh$_4$** without added anion, and shift of resonances in presence of TBA·Cl or TBA·BzO. All spectra recorded at 176 MHz and 293 K at 2.0 mM host in 95:5 CD_3CN:D_2O. Carbon d resonance could not be identified after two equivalents of TBA·BzO due to overlap with a BPh_4^- resonance. All y-axes are 2 ppm high. For a more concentrated ^{13}C NMR spectrum of **1·BPh$_4$** (in d_6-DMSO), see Figure S2.

Molecular Dynamics Simulations

Protocol: The GROMACS MD package (version 5.1.2)[S17] in conjunction with the GROMOS 54A7 force field[S18] was used in all simulations. Water was represented explicitly using the simple point charge (SPC) model.[S19] Parameters for acetonitrile, benzoate and **1**$^+$ were calculated by the automated topology builder.[S20]

Each system was simulated under periodic boundary conditions in a rectangular simulation box. The temperature of the system was maintained by coupling to an external temperature bath at 298 K with a coupling constant of τ_T = 0.1 ps using a velocity rescaling thermostat. The pressure was maintained at 1 bar by weakly coupling the system to a semi-isotropic pressure bath using an isothermal compressibility of 4.5 × 10^{-5} bar^{-1} and a coupling constant of τ_P = 0.5 ps. During the simulations, the length of all bonds was constrained using the LINCS algorithm.[S21] The SETTLE algorithm[S22] was used to constrain the geometry of water molecules. The timestep of each simulation was 2 fs. Electrostatic interactions were calculated using particle mesh Ewald summation and nonbonded interactions were calculated with a cut-off of 1.0 nm. Both were updated each timestep.

Three replicate systems were constructed for simulation, with random starting positions of the solute molecules. Each system consisted of 10 benzoate anions, 10 amidinium cations, 9100 acetonitrile and 1400 water molecules (*i.e.* a concentration of 20 mmol L^{-1}, 10 times the concentration used for ^{13}C NMR experiments, and 20 times the concentration used for ITC experiments, TBA cations and BPh_4^- anions were omitted for simplicity). Each replicate was simulated for 50 ns.

Results: In each simulation, pairing of benzoate and **1**$^+$ molecules occurred spontaneously, and all amidinium or benzoate molecules interacted with one another by the end of the computation. These pairs interact through hydrogen bonding interactions (Figure S32), and no stacking interactions are observed. Some **1·BzO** pairs formed clusters by interacting with adjacent complexes through additional hydrogen bonding interactions involving the “sideways-facing” N–H groups. Sheet-like structures of up to three **1·BzO** pairs were observed, and this packing arrangement is also observed in the SCXRD structure (where the **1·BzO** complexes assemble into a 1D tape through such interactions). Larger aggregates would be expected with scaling up of the MD system size. As would be expected, the hydrogen bonding parts of the molecules (amidinium and carboxylate groups) are largely solvated by water molecules, while the more lipophilic areas of the molecule (aromatic rings, and *tert*-butyl groups) are preferentially solvated by acetonitrile molecules (Figure 1 and S33).

Figure S32. View of the entire simulation at the end of the experiment with solvents omitted for clarity.

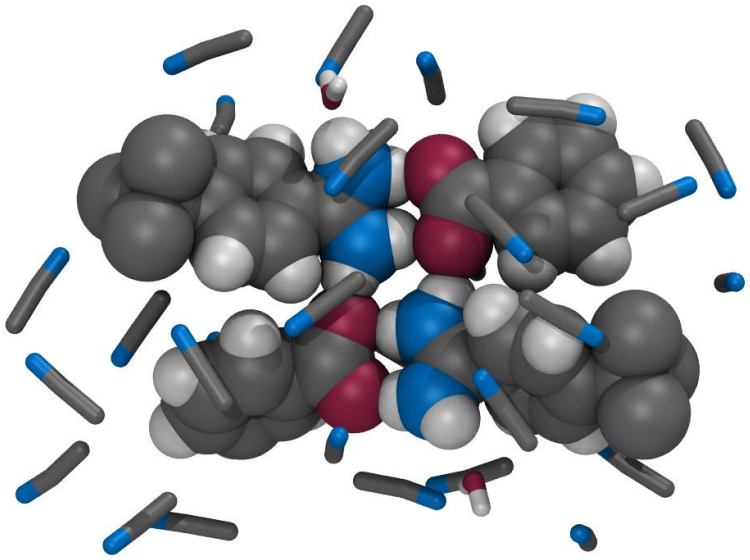

Figure S33. View of one set of amidinium···benzoate complexes at the end of the simulation, showing preferential solvation of different parts of the molecules by acetonitrile or water.

Gas adsorption

The solvent accessible surface (Figure S34) and N_2 accessible surface areas (Table S4) were computed for the crystal structures of *tet*- and *ortho*-[**2**·$(TP)_2$]$_n$ using the "Atoms Volumes & Surfaces" tool in Accelrys Materials Studio 5.0, with a probe diameter of 1.82 Å.[S23] These surfaces revealed that while both materials contain significant pores, in *ortho*-[**2**·$(TP)_2$]$_n$ these pores are disconnected and thus not accessible to nitrogen gas.

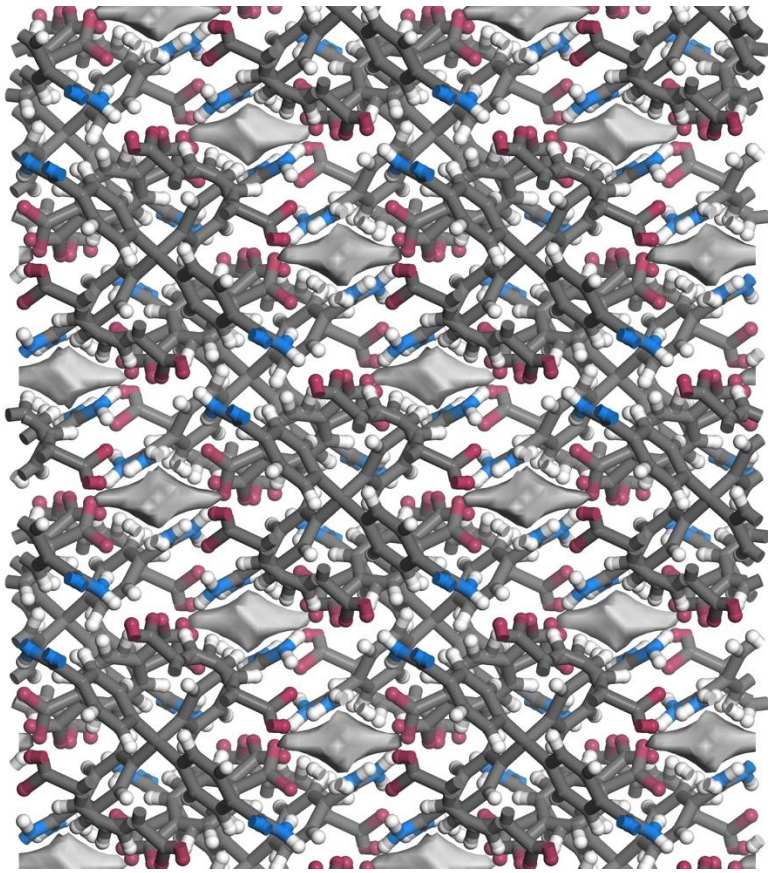

Figure S34. Diagram showing non-continuous pores in structure of *ortho*-[**2**·$(TP)_2$]$_n$.

Table S4: Nitrogen accessible surface areas, pore diameter and density of the desolvated crystal structures. Solvent in *tet*-[**2**·$(TP)_2$]$_n$ was removed during analysis with Accelrys Materials Studio 5.0.[S23]

Material	N_2-accessible surface area (m^2 g^{-1})	Pore diameter (nm)	Density (g cm^{-3})
tet-[**2**·$(TP)_2$]$_n$	1473	1.26	0.82
ortho-[**2**·$(TP)_2$]$_n$	0	–	1.55

While these calculations indicate that *tet*-[**2**·$(TP)_2$]$_n$ has accessible pores, as yet we have been unable to successfully activate the material. Despite using supercritical CO_2 drying and solvent exchange and evaporation methods, no significant nitrogen absorption was observed.

References

[S1] A. J. Lowe, F. M. Pfeffer, *Chem. Commun.* **2008**, 1871.

[S2] B.F. Hoskins, R. Robson, *J. Am. Chem. Soc.* **1989**, *111*, 5962.

[S3] T. J. Zimmerman, T. J. J. Müller, *Synthesis*, **2002**, *9*, 1157.

[S4] A. Petitjean, L. A. Cuccia, M. Schmutz, J.-M. Lehn, *J. Org. Chem.* **2008**, *73*, 2481.

[S5] H. E. Gottlieb, V. Kotlyar, A. Nudelman, *J. Org. Chem.* **1997**, *62*, 7512.

[S6] J. Cosier and A. M. Glazer, *J. Appl. Crystallogr.* **1986**, *19*, 105.

[S7] Agilent Technologies, *CrysAlisPro*, **2011**.

[S8] L. Palatinus, G. Chapuis, *J. Appl. Crystallogr.* **2007**, *40*, 786.

[S9] P. W. Betteridge, J. R. Carruthers, R. I. Cooper, K. Prout, D. J. Watkin, *J. Appl. Crystallogr.* **2003**, *36*, 1487.

[S10] R. I. Cooper, A. L Thompson, D. J. Watkin, *J. Appl. Crystallogr*, **2010**, *43*, 1017.

[S11] R.I. Cooper, R. O. Gould, S. Parsons, D. J. Watkin, *J. Appl. Crystallogr.* **2002**, *35*, 168.

[S12] P. van der Sluis, A. L. Spek, *Acta Crystallogr*. **1990**, *A46*, 194; A. Spek, *J. Appl. Crystallogr*. **2003**, *36*, 7.

[S13] M. Berger, F. P. Schmidtchen, *Angew. Chem. Int. Ed.* **1998**, *37*, 2694.

[S14] P. Thordarson, *Chem. Soc. Rev.* **2011**, *40*, 1305.

[S15] J. L. Sessler, D. E. Gross, W.-S. Cho, V. M. Lynch, F. P. Schmidtchen, G. W. Bates, M. E. Light, P. A. Gale, *J. Am. Chem. Soc.* **2006**, *128*, 12281.

[S16] M. J. Hynes, *J. Chem. Soc., Dalton Trans.* **1993**, 311.

[S17] M. J. Abraham, T. Murtola, R. Schulz, S. Páll, J. C. Smith, B. Hess, E. Lindahl, *SoftwareX*, **2015**, *1–2*, 19.

[S18] N. Schmid, A. P. Eichenberger, A. Choutko, S. Riniker, M. Winger, A. E. Mark, W. F. van Gunsteren, *Eur. Biophys. J.* **2011**, *40*, 843.

[S19] J. Hermans, H. J. C. Berendsen, W. F. van Gunsteren, J. P. M. Postma, *Biopolymers*, **1984**, *23*, 1513.

[S20] A. K. Malde, L. Zuo, M. Breeze, M. Stroet, D. Poger, P. C. Nair, C. Oostenbrink, A. E. Mark, *J. Chem. Theory. Comput.* **2011**, *7*, 4026.

[S21] B. Hess. H. Bekker, H. J. C. Berendsen, J. G. E. M. Fraaije, *J. Comput. Chem.* **1997**, *18*, 1463.

[S22] S. Miyamoto, P. A. Kollman, *J. Comput. Chem.* **1992**, *13*, 952.

[S23] *Materials Studio, version 5.0*, Accelrys Software Inc. San Diego, CA, **2009**.